



# Multi-objective trade-off optimal control of energy management for hybrid system

T. Deng<sup>1,2</sup> · P. Tang<sup>1</sup> · CH. S. Lin<sup>3</sup> · X. Li<sup>1</sup>

Received: 8 September 2017 / Accepted: 21 March 2018 / Published online: 31 March 2018  
© The Brazilian Society of Mechanical Sciences and Engineering 2018

## Abstract

Currently, energy management control mainly focuses on single-objective optimization (SOO). Even if multi-objective optimization (MOO) problem is studied, it is often converted into an SOO problem by using the weighted sum method. Obviously, it cannot really reflect the essential strengths of MOO. In this paper, a parallel hybrid electric vehicle is taken as the research object. The fuel economy, emissions, and drivability performance are taken as optimization objectives. The parameters of energy management and driveline system are optimized. Considering the constraint conditions of the dynamic performance and charge balance, the fast non-dominated sorting differential evolution algorithm (NSDEA) is proposed to solve the multi-objective optimization problem. Then multi-group sets of Pareto solutions with good distribution and convergence are obtained. The simulation results of NSDEA show that the fuel economy is increased by 20.26% on average. The emissions evaluation index is optimized by 11.33% on average, and the maximum carbon monoxide (CO) optimization value reaches 21.9%. The average of drivability evaluation index (jerk) is up to 20.84%, and 40.32% for maximum. Obviously, the above obtained results are discrete points. They only represent some optimal solutions. Based on the above sets, the locally weighted scatter plot smoothing method is used to fit continuous curve and surfaces. Then, the multi-objective Pareto trade-off optimal control surface is established to further obtain the optimal solutions. This study can provide more reference for the optimal control strategy and lay a foundation for multi-objective energy management of the actual vehicle.

**Keywords** Hybrid system · Energy management · Multi-objective · Trade-off · Optimization

## List of symbols

$A_i$	Fitting coefficient of the external characteristic mathematical model
$A_k$	Fitting coefficient matrix of the universal characteristic mathematical model
$cl\_n$	Engagement times of clutch
CR	Crossover probability

$CR_{max}$	Maximum value of the crossover probability
$CR_{min}$	Minimum value of the crossover probability
DN	Equation index of components' action times
$d_{max-min}$	Maximum value among the minimum distance between individual vectors
$d_{min}^i$	Minimum distance between individual $i$ and $j$
$D_i$	Crowding distance
$E$	Rate of pollutant emissions
$E_{CO}$	Emission rate of carbon monoxide (CO)
$E_{HC}$	Emission rate of hydrocarbon (HC)
$E_{NO_x}$	Emission rate of nitrogen oxides ( $NO_x$ )
$f$	$m$ dimensional target vector
$F$	Variation constant
$f_2$	Comprehensive evaluation index of emissions
$fc\_n$	Starting times of engine

Technical Editor: Kátia Lucchesi Cavalca Dedini.

✉ T. Deng  
d82t722@cqjtu.edu.cn

<sup>1</sup> School of Mechatronics and Automotive Engineering, Chongqing Jiaotong University, Chongqing 400074, China

<sup>2</sup> Chongqing Key Laboratory of System Integration and Control for Urban Rail Transit Vehicle, Chongqing 400074, China

<sup>3</sup> School of Mechanical Engineering, Sichuan University of Science and Engineering, Zigong 643000, China

$F(x)$	Target vector	$T_{\text{chg}}$	Preset charging torque (N m)
$F_{\text{min}}$	Minimum value of zoom factor	$T_{\text{chgs}}$	Additional actual charging torque (N m)
$F_{\text{max}}$	Maximum value of zoom factor	$T_{\text{cl}}$	Clutch torque (N m)
$f(U_i^t)$	Target value of test individuals	$T_e$	Engine torque (N m)
$f(X_i^t)$	Fitness value of target individuals	$T_m$	Motor torque (N m)
$f_m^i(\cdot)$	The $m$ th target function of individual $i$	$T_w$	Total of engine and motor torque (N m)
$f_m^j(\cdot)$	The $m$ th target function of individual $j$	$U_i^t$	Test individual
$ f_m^i(x) - f_m^j(x) $	The distance between individual $i$ and $j$	$u_{ij}^t$	The $j$ th gene of individual $i$ of the $t$ th generation
$G$	Current generation number	$v_{ij}^t$	Mutated individual gene
$G_{\text{max}}$	Maximum generation number	$v_i^{t+1}$	The $i$ th variant individual generated by the $t$ th generation
$gb\_j$	Jerk generated by gearbox	$w_1$	Input power of clutch (kW)
$gb\_n$	Shifting times of transmission	$w_2$	Output power of clutch (kW)
$g_e$	Specific fuel consumption	$W$	Weighting coefficient
$g_j$	$j$ dimensional inequality constraint vectors	$x$	Decision space
$h_k$	$k$ dimensional equality constraint vectors	$x_{\text{min}}$	Minimum value of the optimized vector
$i$	Order of engine speed variable for engine torque fitting	$x_{\text{max}}$	Maximum value of the optimized vector
$j$	Order of engine speed fitting	$x_{r1}^t$	The target individual 1 of the $t$ th generation
$k$	Fitting order	$x_{r2}^t$	The target individual 2 of the $t$ th generation
$k_2$	Fitting coefficient matrix of emission characteristic for pollutants	$x_{r3}^t$	The target individual 3 of the $t$ th generation
$k(t)$	The gear ratio of transmission	$x_{ij}^t$	Target individual gene
$l$	Order of engine speed variable for universal characteristic fitting	$X_i^t$	Target individual
$m$	The number of target vectors	$X_i^{t+1}$	Selected individual
$n$	the number of decision variables which constitute $x$ decision space	$y$	Objective evaluation index
$n_e$	Engine speed (r/min)	$\eta_c$	Charger efficiency
$n_m$	Motor speed (r/min)	$\eta_d$	Final drive efficiency
$n_w$	Wheel speed (r/min)	$\eta_e$	Engine efficiency
$N_p$	Population number	$\eta_m$	Motor efficiency
$N_{\text{obj}}$	Target number	$\eta_t$	Transmission efficiency
$N$	Population size		
$P_m$	Motor power (kW)		
$P_e$	Engine power (kW)		
$P_w$	Vehicle power (kW)		
$\rho_m$	Motor speed ratio		
$\rho(k(t))$	Total drive ratio of the corresponding gears		
$Q_{\text{CO}}$	Emission amount of CO pollutant (g/L)		
$Q_{\text{HC}}$	Emission amount of HC pollutant (g/L)		
$Q_{\text{NO}_x}$	Emission amount of NO <sub>x</sub> pollutant (g/L)		
$Q_{\text{fc}}$	Fuel consumption of the engine (L/100 km)		
$\text{rand}_{ij}$	The random number of corresponding genes		
$s$	Model order		
$\text{sgn}$	Symbol function		
$\text{SOC}$	State of charge		
$\text{SOC}_{\text{max}}$	Maximum value of SOC		
$\text{SOC}_{\text{min}}$	Minimum value of SOC		
$t$	Driving time (s)		
$T$	Required torque (N m)		

## 1 Introduction

Hybrid electric vehicle (HEV) can achieve optimal energy consumption through controlling the reasonable power distribution of the engine and motor. The key to its performance is the energy management control strategy. Currently, most researches mainly focus on fuel economy, but pay less attention to emission and drivability for energy management control, for example, some instantaneous optimization algorithms such as SOC closed loop control strategy [1], equivalent consumption minimization strategies (ECMS) [2], real-time control strategy based on approximate minimum principle [3], and global optimization methods such as dynamic programming (DP) [4] and stochastic dynamic programming (SDP) [5]. Both of them

were proposed to enhance fuel economy for HEV energy management control. However, emission and drivability performance also have significant impact on energy management [6–8]. In view of this, some scholars considered trade-off control between fuel economy and emission [9–13]. A few scholars further considered drivability as the suboptimal parameter for energy management based on optimization of fuel economy and emission [14–17]. But they mainly adopted weighted sum method to deal with the trade-off control for the multi-objective optimization problem. Essentially, weighted sum method may hide the real situation of each target and cannot reflect the coupling relation between different targets [18]. Obviously, it still belongs to a single-objective optimization algorithm. Actually, the results of multi-objective optimization problem should be mutually independent and balanced. The performance optimization of one single target may inevitably damage the other targets. The optimization results should be multiple sets of solutions rather than a single optimal solution. Unfortunately, current control strategies rarely follow this essential characteristic of multi-objective problem. As a result, the dimension of optimization targets are reduced, and the mapping relationship between independent variables and objective targets is weakened.

As we know, the theory of Pareto optimality is very good at solving the multi-objective optimization problem. It can better reflect the essential characteristic of the multi-objective problem. Therefore, the evolutionary algorithm based on Pareto principle is proposed to solve the multi-objective optimization problem. A group of non-inferior Pareto solution sets is obtained to overcome the shortcomings of traditional weighting methods. However, not only the Pareto optimality, but also the evolutionary algorithm needs a great deal of iterative calculation. So, the locally weighted scatter plot smoothing (LOWESS) method is adopted to fit the obtained optimal discrete points into continuous surfaces. Then they are used to establish the trade-off control curve surfaces of HEV and the existence of the optimal solution sets is further studied.

## 2 Parallel hybrid electric vehicle (PHEV)

A typical parallel hybrid electric vehicle (PHEV) is taken as the studied object. The structure of PHEV is shown in Fig. 1. The main parameters of PHEV are illustrated in Table 1.

### 2.1 Working modes of PHEV

The working modes of PHEV include pure electric driving mode, engine driving alone mode, combined driving mode of engine and assisted motor, charging mode and regenerative

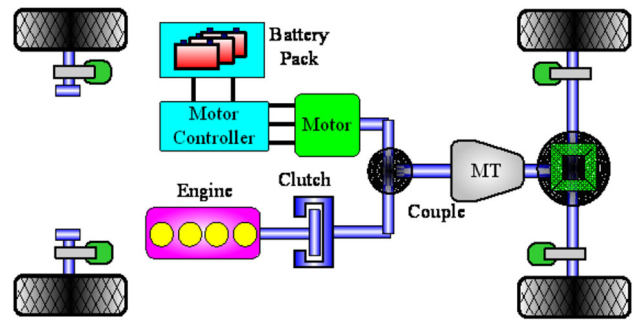


Fig. 1 The structure of the parallel hybrid electric vehicle

braking mode. The relationships between power, torque and speed under each working mode are as follows.

#### 2.1.1 Pure electric driving mode

Under this mode, the required power is small. The motor can drive the vehicle alone. The relationships between torque and speed are as shown as follows:

$$\begin{cases} n_w(t) = n_m(t)/\rho_m \\ T_w(t) = \rho_m T_m(t) \\ P_w(t) = \eta_m \eta_t \eta_d P_m(t) \end{cases} \quad (1)$$

#### 2.1.2 Engine driving alone mode

Under this condition, the engine drives the vehicle alone. Namely, the engine provides all the required power alone. The engine can be controlled to work within the optimal working region:

$$\begin{cases} n_w(t) = n_e(t)/\rho(k(t)) \\ T_w(t) = p(k(t))T_e(t) \\ P_w(t) = \eta_e \eta_t \eta_d P_e(t) \end{cases} \quad (2)$$

#### 2.1.3 Combined driving mode of engine and assisted motor

At this moment, both the engine and motor work together to drive the vehicle. However, the engine provides the main driving force, while the motor only provides the auxiliary power:

$$\begin{cases} n_w(t) = n_e(t)/\rho(k(t)) = n_m(t)/\rho_m \\ T_w(t) = p(k(t))T_e(t) + \rho_m T_m(t) \\ P_w(t) = \eta_e \eta_t \eta_d P_e(t) + \eta_m \eta_t \eta_d P_m(t) \end{cases} \quad (3)$$

#### 2.1.4 Charging mode

Right now, the vehicle runs with light load. The provided power of the engine exceeds the required power of the

**Table 1** Main parameters of PHEV

Component	Parameter	Value
Entire vehicle	Curb weight (kg)	1200
	Total mass (kg)	1600
	Length × breadth × height (m)	4.41 × 1.75 × 1.64
	Wheel base (m)	2.6
Engine	Displacement (L)	1.0
	Rated power (kW/(r/min))	41/5700
	Max torque ((N m)/(r/min))	81/3477
Motor	Max power (kW)	75
	Max speed (r/min)	10,000
Transmission	Type	MT
	Ratio range	0.75–3.56
Battery	Type	Lead-acid battery
	Nominal voltage (V)	308
	Nominal capacity of unit (Ah)	26

entire vehicle. The SOC of the battery is lower. At this moment, the engine not only provides the required power for the entire vehicle, but also can charge the battery through a generator and power converter. When the SOC reaches the predefined threshold value, the battery is not charged. Namely, the engine stops charging:

$$\begin{cases} n_w(t) = n_e(t)/\rho(k(t)) = n_m(t)/\rho_m \\ T_w(t) = p(k(t))T_e(t) - \rho_m T_m(t) \\ P_w(t)/(\eta_t \eta_d) = \eta_e P_e(t) - P_m(t)/\eta_c \end{cases} \quad (4)$$

### 2.1.5 Regenerative braking mode

When the vehicle decelerates or brakes, the motor works as a generator to charge the battery through the power converter:

$$\begin{cases} n_w(t) = n_m(t)/\rho_m \\ T_w(t) = \rho_m T_m(t) \\ P_w(t)\eta_t \eta_d \eta_c = P_m(t) \end{cases} \quad (5)$$

## 2.2 Electric-assisted control strategy for PHEV

In this paper, we mainly focus on the multi-objective optimization (MOO) algorithm and pay less attention to the control strategy. Thus, the typical parallel electric-assisted control strategy is adopted to verify the proposed MOO algorithm. The working principle of the electric-assisted control strategy is illustrated in Fig. 2.

The parameter SOC<sub>min</sub> means lower limit value of SOC, which should be predefined to avoid overcharging and overdischarging. The detailed control rules of electric-assisted control strategy are described as follows.

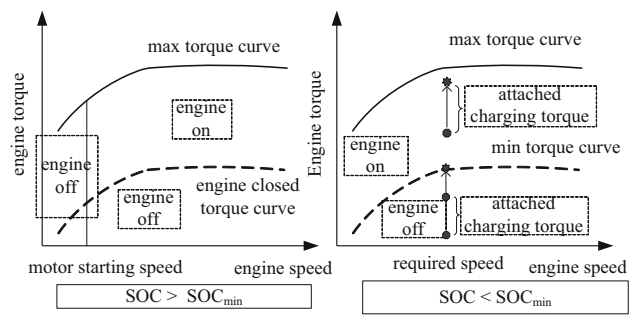


**Fig. 2** Parallel electric-assisted control strategy

1. When the SOC is below the lower limit value (SOC < SOC<sub>min</sub>), the battery needs to be charged. That means the engine not only provides power for the vehicle, but also charges the battery through the motor/generator.
2. When the SOC is larger than the lower limit value (SOC > SOC<sub>min</sub>), the required torque should be between the maximum torque and the engine closing torque.
3. If the required speed is lower than the engine idling speed, the engine is closed and the motor works alone to start the vehicle.
4. If the required speed is greater than the idling speed and the required torque is smaller than the engine maximum torque, the engine works alone.
5. Otherwise, the motor starts working to supply the auxiliary power.

The relationship of different torques is shown as follows:

$$T = T_m + T_e. \quad (6)$$

When the SOC is smaller than the lower limit value ( $SOC < SOC_{min}$ ), the battery needs to be charged. At this moment, there are two modes. If the required driving torque is between the minimum and maximum engine torque, an additional actual charging torque  $T_{chgs}$  will be generated. The attached charging torque is proportional to  $[0.5 * (SOC_{max} + SOC_{min}) - SOC]$  [19], as shown in Eq. (7).  $T_{chg}$  is the preset charging torque in the simulation model according to engineering experiences. In this paper, we adopt the preset value in Advisor simulation platform. When the SOC is small, the battery is forced to charge. At this moment, the preset charging torque  $T_{chg}$  is firstly used to charge the battery. Then the actual attached charging torque  $T_{chgs}$  is obtained to charge the battery according to the SOC variation. When the SOC is lower, the battery needs to be quickly charged. That means the actual attached charging torque should be larger. If the required driving torque is less than the minimum torque of the engine, the attached torque is used to charge the battery. No matter what the condition may be, the engine torque is equal to the sum of the generated charging torque and the required torque of the entire vehicle. If the sum is too small, the engine will run along with the minimum working curve. The relationships of different torques are illustrated as follows:

$$\begin{cases} T = T_e - T_{chgs} \\ T_{chgs} = T_{chg} \times \left[ \frac{(SOC_{max} + SOC_{min})}{2} - SOC \right] \end{cases} \quad (7)$$

### 3 Multi-objective optimization (MOO) algorithm for energy management of HEV

#### 3.1 MOO problem

Compared with the general optimization problem, the MOO problem has many optimized objectives. Any decision variable may influence any optimization target. Taking the typical minimum optimization for example, the MOO problem can be described with target vectors, equality and inequality constraint vectors, and  $n$  dimensional decision variables:

$$\begin{aligned} \min \quad & y = f(x) = (f_1(x), \dots, f_m(x)) \\ \text{s.t.} \quad & g_j(x) \leq 0 \quad j = 1, 2, \dots, j \\ & h_k(x) = 0 \quad k = 1, 2, \dots, k \\ \text{d.v.} \quad & x = [x_1, x_2, x_3, \dots, x_n]. \end{aligned} \quad (8)$$

Obviously, the essential MOO problem is to solve the mapping relationship of function. The mapping relationship between the decision space and the objective space is not the common one-to-one relationship. There also exists

a mapping relationship between each independent variable of decision space and each target of objective space. In other words, the mapping relationship between the decision space and objective space belongs to a complex many-to-many relationship. Therefore, the solution set of the multi-objective problem belongs to vector optimization in nature. As we know, the vector sets are different in order relations. The solution set can be divided into absolute optimal solution, strong efficient solution, more efficient solution, fuzzy efficient solution, satisfactory solution, Pareto optimal solutions and other solutions. Among them, the Pareto optimal solution is the best solution of the multi-objective mapping relation.

#### 3.2 MOO mathematical modeling

##### 3.2.1 Establishment of optimization targets

According to the multi-objective principle, the mathematical models for fuel economy, emission and drivability are established as follows:

##### 1. Fuel economy

In general, the simulation and calculation of fuel economy and pollutants emission is based on the mathematical model of the engine. According to the experimental data of the engine under steady-state conditions, the external characteristic model and universal characteristic model of the engine are established as follows [19]:

$$\begin{cases} g_e = \sum_{j=0}^s \sum_{l=0}^j A_k T_e^l n_e^{j-l} \\ T_e = \sum_i^k A_i n_e^i \\ k = (j + 1) \times (j + 2) - j - 1 + i \end{cases} \quad (9)$$

The fuel consumption of the engine can be calculated according to the above obtained effective specific fuel consumption [20]:

$$Q_{fc} = \int_0^t g_e(n_e(i), T_e(i)) P_e(i) d_i \quad (10)$$

The evaluation index of fuel economy is defined as follows:

$$f_1(x) = Q_{fc}(x) \quad (11)$$

##### 2. Emission

In the same way, the universal characteristic model of emission also can be gained according to the experimental data of emission test. The emission characteristic of pollutants is calculated as follows [19]:



$$E = \sum_{j=0}^s \sum_{l=0}^j k_2 \left[ \frac{1}{2}(j+1)(j+2) - j - 1 - l \right] T_e^l n_e^{j-l}. \quad (12)$$

For gasoline engine, the pollutants mainly include CO, HC and NO<sub>x</sub>. So we only consider the three pollutants as evaluation indexes of emission. The emission amount of pollutant can be computed as follows:

$$\begin{cases} Q_{CO} = \int_0^t E_{CO}(n_e(i), T_e(i)) di \\ Q_{HC} = \int_0^t E_{HC}(n_e(i), T_e(i)) di \\ Q_{NO_x} = \int_0^t E_{NO_x}(n_e(i), T_e(i)) di \end{cases} \quad (13)$$

According to existing experimental data and emission characteristics, we find that the CO value is almost an order of magnitude bigger than the other two indexes. We adopt the normalization method to deal with orders of magnitude for the three objectives [21]. We enlarge ten times the HC and NO<sub>x</sub> so as to be of the same magnitude as the CO index. Then the comprehensive evaluation index of emission can be illustrated as follows:

$$f_2(x) = 10 \times Q_{HC}(x) + 10 \times Q_{NO_x}(x) + Q_{CO}(x). \quad (14)$$

### 3. Drivability

It is hard to objectively reflect the real drivability with subjective evaluation methods. Therefore, the objective indexes closely related with fuel economy and emission are selected as evaluation indexes of drivability, such as jerk, slipping work, tip-in/out response, and times of key components. The comprehensive evaluation of drivability is built as follows:

$$\begin{cases} f_3 = gb\_j + W + DN \\ gb\_j = \int_0^{t_s} j(t) dt \\ W = \int_{t_1}^{t_2} T_{cl}(w_1 - w_2) dt \\ DN = w_1 * fc\_n + w_2 * gb\_n + w_3 * cl\_n \end{cases} \quad (15)$$

Obviously, drivability contains many evaluation indexes. Some indexes are hard to obtain. In this paper, we only choose jerk as the evaluation index of drivability. The MOO problem is as follows:

$$f_3 = gb\_j. \quad (16)$$

### 4. Multi-objective evaluation model

The evaluation mode of MOO is built as follows:

$$\min y = F(x) = (f_1(x), f_2(x), f_3(x)). \quad (17)$$

As we know, there are many parameters which can influence fuel economy, emission and drivability. If all

parameters are designed to be optimized, the optimization process will be very complicated. Therefore, it is crucial to select suitable parameters for optimization. In this paper, we select the parameters of control strategy and powertrain as optimized targets, which significantly influence optimization according to the past experiments and experiences. Some evaluation indexes of drivability, which is most closely to fuel economy and emission, are also selected. The specific parameters are as shown in Table 2. The maximum engine power not only embodies the dynamic performance and fuel economy, but also influences the drivability. Similarly, the overload coefficient and gear ratio of motor can also affect the fuel economy and drivability. Battery is a very important component of HEV. Its parameters directly influence the fuel economy, emission and drivability performance of HEV, such as battery block number, upper limit of electric quantity for battery, lower limit of electric quantity for battery and battery charging torque. In addition, some control parameters such as minimum engine torque coefficient, engine closing coefficient, lower limit of engine speed and initial temperature for three way catalytic converter (TWC) directly affect the fuel economy and emission performance.

Then, the constrain condition of the dynamic performance and battery charge balance are treated as the constrain conditions, as shown in Table 3.

Thus, the mathematical model of MOO problem is established as follows:

$$\begin{aligned} \min y &= F(x) = (f_1(x), f_2(x), f_3(x)) \\ f_1(x) &= Q_{fc}(x) \\ f_2(x) &= 10Q_{HC}(x) + 10Q_{NO_x}(x) + Q_{CO}(x) \\ f_3(x) &= gb\_j \\ \text{s.t. } g_j(x) &\leq 0, \quad j = 1, 2, \dots, J. \end{aligned} \quad (18)$$

#### 3.2.2 MOO simulation model

According to Eq. (18), the simulation model of MOO based on Advisor platform is established, as shown in Fig. 3. The model includes engine model, emission after treatment model, clutch model, torque coupler model, transmission model, final drive model, wheel model, battery pack model, motor model, control system model and so on.

## 4 MOO algorithm for PHEV energy management

For the MOO problem, it is difficult to directly judge the merits and demerits of each individual. It needs a comprehensive index to evaluate all objectives. Fast non-dominated sorting genetic algorithm-II (NSGA-II) can

**Table 2** Optimization parameters

Type	Parameter	Range
Powertrain	Maximum engine power (kW)	$P_e \in [20, 50]$
	Motor overload coefficient	$R_o \in [1, 3]$
	Final drive	$F_d \in [0.55, 0.9]$
Control strategy	Battery block number (block)	$N_b \in \{15, 16 \dots 50\}$
	Upper limit of electric quantity for battery (%)	$H_{soc} \in [0.55, 0.9]$
	Lower limit of electric quantity for battery (%)	$L_{soc} \in [0.1, 0.55]$
	Battery charging torque (N m)	$T_{chg} \in [10, 30]$
	Minimum engine torque coefficient	$K_{min} \in [0.4, 1]$
	Engine closing coefficient	$T_{off} \in [0, 0.5]$
	Initial temperature for TWC (°C)	$EX_t \in [10, 30]$
	Lower limit of engine speed (r/min)	$N_n \in [80, 110]$

**Table 3** Constraint conditions

Constraint condition	Description	Range	
Dynamic performance	Acceleration	Acceleration time from 0 to 100 km/h	$\leq 14$ s
		Acceleration time from 40 to 100 km/h	$\leq 10$ s
	Gradient	Gradient	$\geq 30\%$
Battery charge balance	The difference of state of charge before and after the cycle	$\leq 0.5\%$	

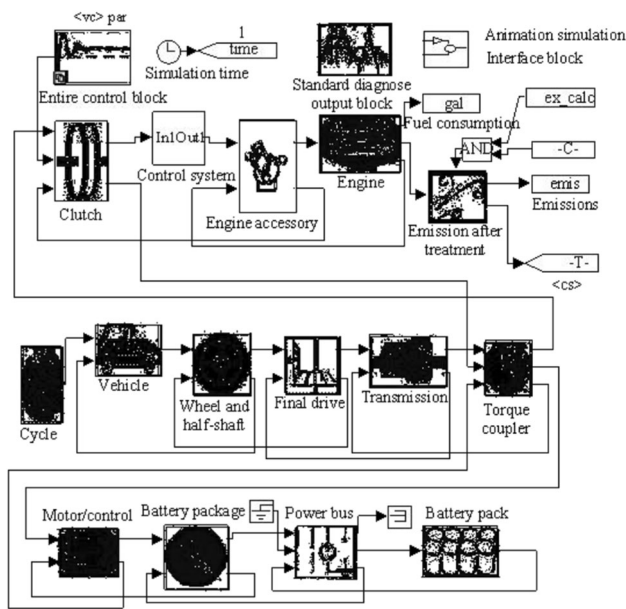


**Fig. 3** Simulation model for the MOO problem

build solution sets with fast non-dominated sorting and crowd distance computing method. In addition, the most prominent evolutionary algorithm is differential evolution (DE) algorithm in recent years. It is an adaptive global optimization algorithm. Compared with typical genetic algorithm (GA), DE has better performance such as faster convergence speed, better convergence effect, better robustness and adaptive ability. Therefore, we propose a

non-dominated sorting differential evolution algorithm (NSDEA) based on NSGA-II and DE algorithm.

### 4.1 Non-dominated sorting differential evolution algorithm (NSDEA)

#### 4.1.1 The characteristics of NSDEA structural solutions

1. Fast hierarchical non-dominated sorting

The target vectors of each individual are compared. The non-dominated individuals of the whole population are identified and then listed as the first layer. The same operation is performed for the remaining population. The non-dominated individuals within residual population are identified as the second layers. Similarly, when the sorting operations are completed for all individuals, the obtained layer number represents the quality of the individual.

2. Method for maintaining population distribution and diversity

The crowding distance which reflects the individual distribution is improved as follows:

$$D_i = \sum_{j=1, j \neq i}^{N_p} \text{sgn} \left( d_{\max-\min} - \sum_{m=1}^{N_{obj}} |f_m^i(x) - f_m^j(x)| \right). \quad (19)$$

It can be further revised as follows. The mutual relationships between multiple indexes are converted into the evaluation indexes, which follow Pareto optimal principle and achieve multi-objective evaluation:

$$\begin{cases} d_{\max-\min} = \max\{d_{\min}^1, d_{\min}^2, \dots, d_{\min}^n\} \\ d_{\min}^i = \min \sum_{m=1}^{N_{\text{obj}}} |f_m^i(x) - f_m^j(x)| \end{cases} \quad (20)$$

### 4.1.2 Analysis of differential evolution algorithm

#### 1. Population initialization

The initial individual of  $N$  population size is randomly generated within the feasible region:

$$X = \{x_1, x_2, \dots, x_N | x_{\min} \leq x \leq x_{\max}\}. \quad (21)$$

#### 2. Mutation

According to individual difference information, the population individual is performed by mutation operation:

$$v_i^{t+1} = x_{r1}^t + F \cdot (x_{r2}^t - x_{r3}^t). \quad (22)$$

#### 3. Crossover

The test individual is decided to be variation individual or target individual through crossover probability:

$$u_{ij}^t = \begin{cases} v_{ij}^t & \text{rand}_{ij} < CR \\ x_{ij}^t & \text{others} \end{cases} \quad (23)$$

#### 4. Selection

The excellent individuals are selected as new population from test individuals and target individuals with greedy strategy:

$$X_i^{t+1} = \begin{cases} U_i^t & f(U_i^t) \leq f(X_i^t) \\ X_i^t & \text{others} \end{cases} \quad (24)$$

Obviously, population number, coefficient of variation and crossover probability are the key control parameters of the DE algorithm. The population number is generally set according to experience, which has small impact on the performance of the DE algorithm. However, the coefficient of variation and crossover probability greatly affect the ability of the global and local search for the population. Therefore, it is difficult to set the values. In this paper, we build a function of adaptive variation to solve the parameter sets as follows:

$$\begin{cases} F = F_{\min} + \frac{(F_{\max} - F_{\min}) \times G}{1 - G/G_{\max}} \\ CR = CR_{\min} + \frac{(CR_{\max} - CR_{\min}) \times G}{1 - G/G_{\max}} \end{cases} \quad (25)$$

Then, the multi-objective optimization algorithm NSDEA is established as shown in Fig. 4.

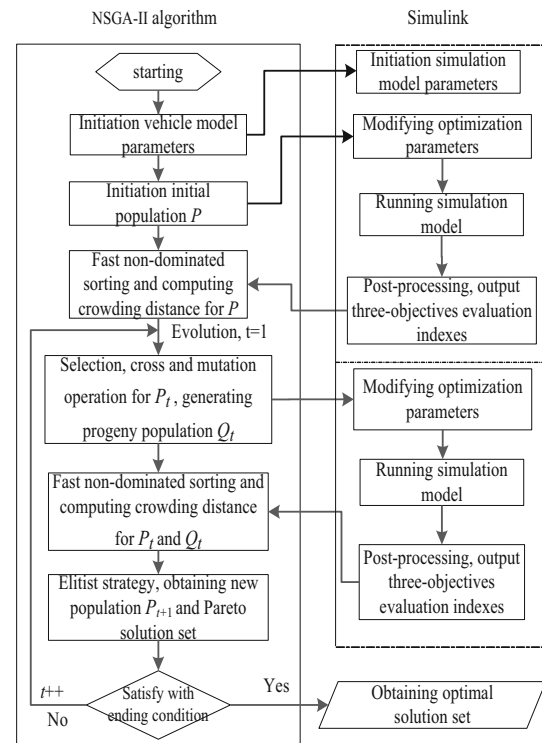


Fig. 4 The HEV-NSGA-II optimization algorithm processes

### 4.2 Simulation analysis of NSDEA

Under urban dynamometer driving schedule (UDDS) cycle, population value, maximum generation value, maximum and minimum value of crossover probability, and maximum and minimum value of mutation probability are set to be 40, 100, 0.7, 0.3, 0.9 and 0.5, respectively. Then, the NSDEA algorithm is embedded into the above established MOO simulation model. Multi-groups of Pareto optimal solution sets can be obtained. The ten most representative groups are selected to analyze, as shown in Table 4. The 11th group represents the setting value and performance index before optimization. The indexes from the 2nd row to the 12th row indicate the optimized parameters. The meanings of variables have been illustrated in Table 2. The parameters of the last six rows stand for the results of optimization.

Obviously, the 10 groups of Pareto optimal solutions are optimized compared with the 11th group. For fuel economy, the average optimization index increases by 20.30% and the maximum value enhances by 22.30%. For drivability, the average optimization performance increases by 20.84% and the maximum value reaches 40.32%. For emission, the comprehensive performance index increases by 9.16% on average.  $Q_{HC}$ ,  $Q_{NO_x}$  and  $Q_{CO}$  increase by 7.24, 8.25 and 13.36%, respectively. The specific optimization indexes are shown in Table 5.



**Table 4** Optimal results and optimized parameter values

No.	$P_e$ (kW)	$N_b$ (block)	$F_d$	$H_{soc}$ (%)	$L_{soc}$ (%)	$T_{chg}$ (N m)	$K_{min}$	$T_{off}$
1	68.71	18	1.16	0.68	0.40	21.73	0.87	0.18
2	68.96	18	1.29	0.66	0.37	22.44	0.95	0.20
3	67.04	17	1.44	0.66	0.36	22.69	0.96	0.21
4	64.35	17	1.31	0.67	0.40	22.29	0.90	0.21
5	65.11	17	1.15	0.67	0.43	22.11	0.88	0.20
6	69.95	20	1.18	0.70	0.37	21.48	0.85	0.17
7	70.00	19	1.17	0.70	0.41	21.46	0.85	0.16
8	65.55	17	1.45	0.66	0.36	22.69	0.96	0.21
9	45.17	17	1.91	0.79	0.21	20.24	0.59	0.24
10	41.43	15	2.50	0.64	0.10	23.04	1.00	0.22
11	41.01	2	1.00	0.70	0.60	15.25	0.40	0.00

$EX_r$ (°C)	$N_n$ (km/h)	$R_o$	$Q_{HC}$ (g/km)	$Q_{NO_x}$ (g/km)	$Q_{CO}$ (g/km)	$f_1$ (g/km)	$f_2$ (L/km)	$f_3$ (m/s <sup>3</sup> )
14.24	80.00	2.53	0.37	0.33	2.09	6.05	9.15	165.53
15.01	80.00	2.56	0.37	0.32	2.62	5.84	9.47	159.34
15.38	80.00	2.55	0.37	0.33	2.23	5.95	9.29	195.48
14.35	80.00	2.59	0.37	0.32	2.71	5.93	9.66	157.54
14.23	80.00	2.65	0.37	0.33	2.13	5.96	9.19	164.27
14.21	81.23	2.42	0.37	0.33	2.07	6.14	9.15	165.53
14.20	81.29	2.46	0.37	0.33	2.04	6.10	9.06	166.48
15.53	80.02	2.53	0.37	0.33	2.22	5.94	9.28	194.67
14.31	91.02	1.52	0.38	0.38	2.98	6.34	10.62	147.87
19.98	80.00	1.87	0.47	0.40	7.65	12.51	16.36	129.01
20.00	99.48	1.80	0.40	0.36	2.61	7.51	10.22	216.16

To illustrate the rationality of the obtained Pareto optimal solution sets, one of the Pareto solution sets is selected to further analyze vehicle performance.

As shown in Fig. 5, the actual speed can accurately follow the required speed with a small error, which meets the speed requirement under the UDDS cycle.

As shown in Fig. 6, the error of SOC at the beginning and end of simulation is less than 0.5%. The amplitude of SOC fluctuation is also small (the maximum value is less than 0.005). The SOC change curve is reasonable.

As shown in Fig. 7, the engine and motor can coordinate well with each other and the power variations can meet the vehicle requirement.

The efficiency of the engine and motor before and after the optimization is comparatively analyzed as shown in Figs. 8 and 9, respectively. It can be seen that the distribution for engine working points has changed a lot. After optimization, the working points of engine within the low-

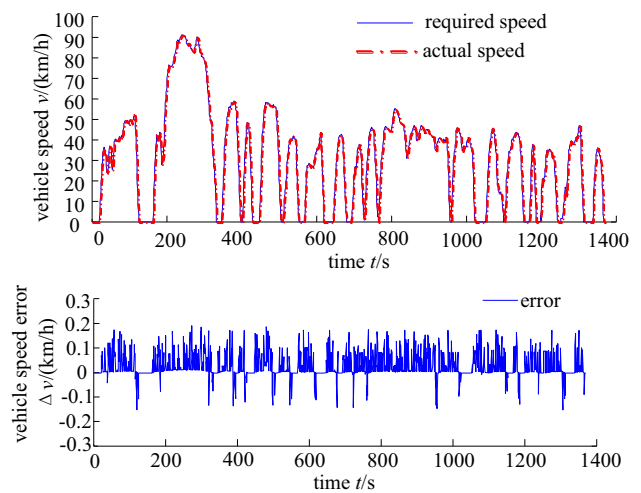


**Fig. 5** Cycle following condition

**Table 5** Optimization indexes

Index	$Q_{HC}$	$Q_{NO_x}$	$Q_{CO}$	$f_1$	$f_2$	$f_3$
Max optimization ratio (%)	7.33	11.89	21.90	22.30	11.33	40.32
Average optimization ratio (%)	7.24	8.25	13.36	20.26	9.16	20.84

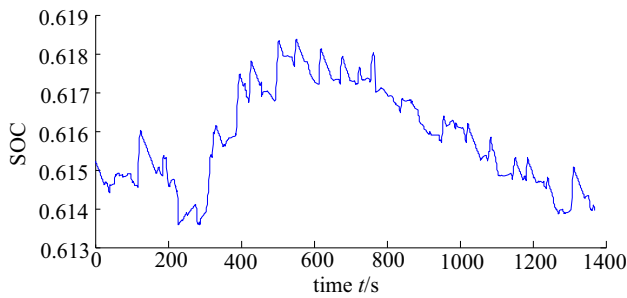


Fig. 6 SOC variation

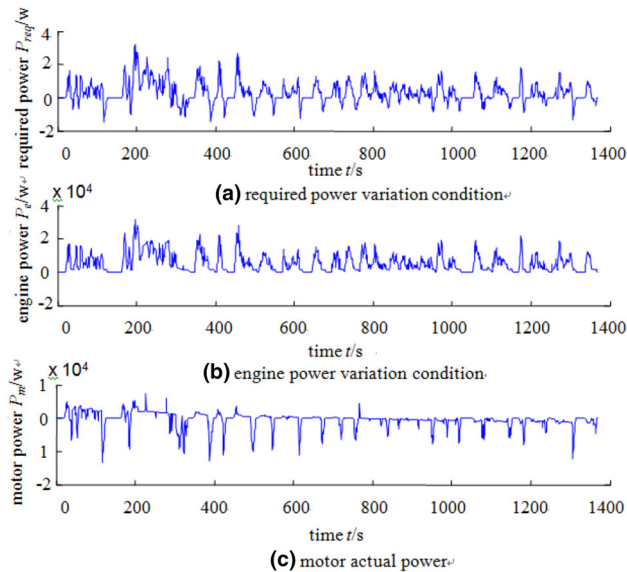


Fig. 7 The power variation

efficient region are obviously reduced. Those points within the high-efficient area are greatly increased. Obviously, fuel economy is significantly improved. The main reason is that the control strategy only regards the fuel economy as the single control target before optimization. Of course, it only reduces fuel consumption, but cannot apparently decrease emission. As we know, the low fuel consumption

Fig. 8 The distribution of engine efficiency points

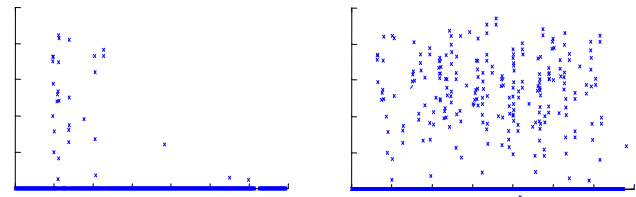
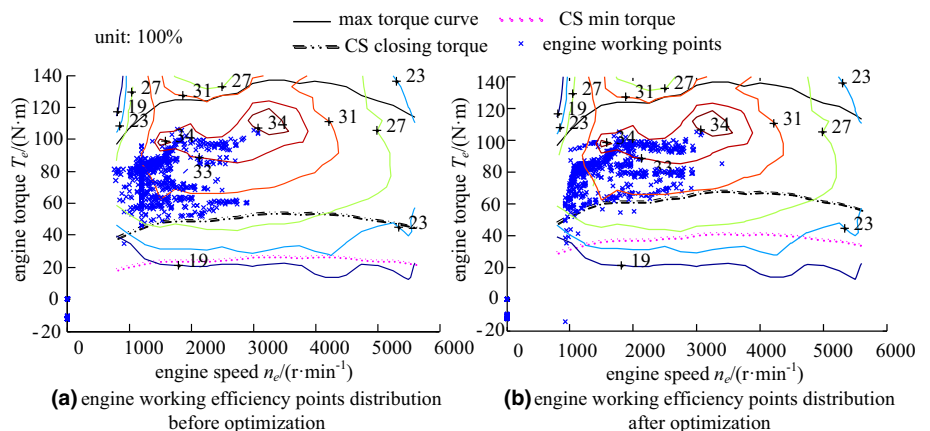
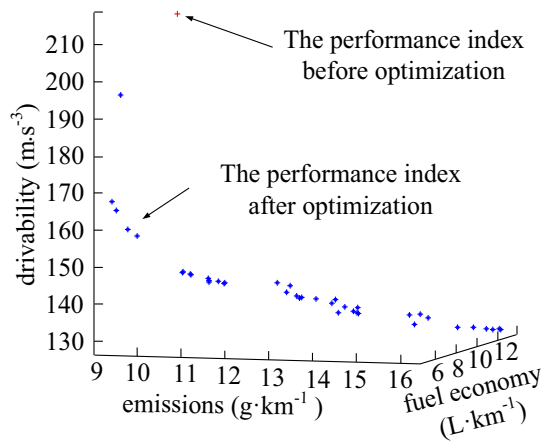


Fig. 9 The distribution of motor efficiency points

region of engine is not consistent with the low emission area and there exists obvious conflicting relationship between fuel economy and emission. In addition, drivability is also in conflict with fuel economy and emission. Furthermore, the enhancement of high-efficient working points for motor after optimization is another factor. Therefore, only by comprehensively considering fuel economy, emission and drivability, trade-off optimization distribution points of engine and motor can be obtained.

According to the above analysis, the obtained optimal solution sets can meet the design requirements of HEV. To further reflect the distribution of each objective from optimization results, 40 groups of Pareto optimal solution sets are plotted and analyzed, as shown in Fig. 10. The selected 40 groups of solution sets are the final Pareto optimal solution sets obtained by simulation. For those sets, there may be a phenomenon that another objective is deteriorated when one objective is optimized. However, it will not happen for the former ten groups of solution sets. It can be concluded from Fig. 10 that the fuel economy, emission and drivability are all optimized. There also exists a conflicting relationship between the three objectives for optimal solution sets, namely, another objective is deteriorated when one objective is optimized.

To show the conflicting relationship between the three objectives more clearly, Fig. 10 can be converted into a two-dimensional map for analysis. As shown in Fig. 11, the evaluation indexes of drivability and fuel economy are comparatively analyzed. The red “+” expresses



**Fig. 10** The trade-off control solutions of comprehensive index

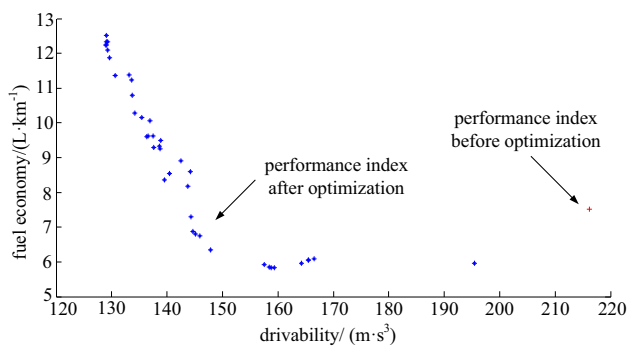


**Fig. 11** The distribution map of drivability and fuel economy solution sets

performance index before optimization, while the blue “\*” indicates the performance index after optimization. Compared with the performance before optimization, the fuel economy and emission are improved for most optimal points. For a few points, fuel economy deteriorates as a result of further optimization of drivability. In the pursuit of extreme drivability, the engine even may run along with the deteriorated points of fuel economy.

As shown in Fig. 12, the evaluation indexes of drivability and emission are analyzed. After optimization, drivability is improved, but emission performance shows partial deterioration.

As shown in Fig. 13, the evaluation indexes of fuel economy and emission are analyzed. After optimization, the most optimal points of fuel economy are improved, while a few points have deteriorated due to the influence of drivability.

Although there is a conflicting relationship among the three objectives, the trade-off optimal solution sets for the multi-objective problem can be obtained according to the above distribution maps.

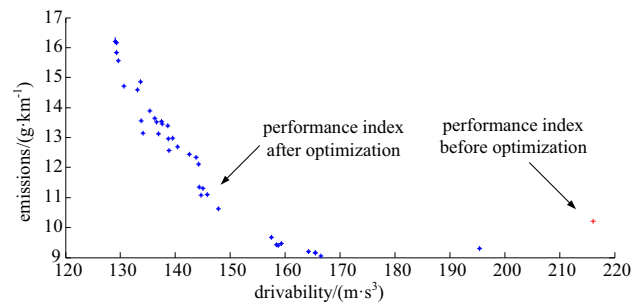


**Fig. 12** The distribution map of drivability and emission solution sets

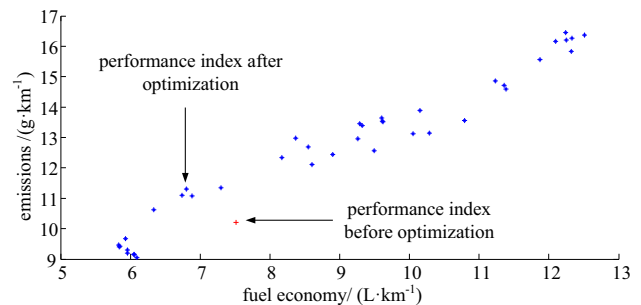


**Fig. 13** The distribution map of fuel economy and emission solution sets

## 5 Pareto trade-off optimal control surface

The above obtained Pareto optimal solution sets consist of a series of discrete points. To obtain more points, it needs more substantial calculation, which causes more complex operations. Therefore, we can adopt interpolation fitting method to fit the discrete optimal points into the optimal surface. When the optimization range contains all regions, the corresponding results should also contain the range of all solutions. For interpolation fitting, all solution sets can be expressed with finite results. Obviously, curved surface fitting is the further utilization and mining of the discrete solution sets. The results of surface fitting are not accurate, but close to the real solutions. Sometimes, this optimal solution may not exist, but we have maximum possibility to search the optimal solution by further excavating results.

For curved surface fitting, the analytical relationship between data is established according to the limited data obtained by the experiment. There are many methods for curved surface fitting, such as least squares method, COONS surface fitting, cubic spline interpolation and artificial neural network. The locally weighted scatter plot smoothing (LOWESS) is a non-parametric fitting method. There is no need to know the dependent variables and independent variables. It can fit the smooth surface with some given data. Moreover, LOWESS has good robustness to deal with the poor fitting effect condition. Therefore, we adopt the LOWESS method to fit the curved surface.

## 5.1 Surface fitting and result analysis

According to the former 40 groups of the Pareto optimal solution sets, the corresponding trade-off control curved surface for fuel economy, emission and drivability can be obtained. The relationship between the three objectives can be further explored. However, there are many optimized variables. The target function also includes three variables. If fitting all the optimized variables and target variables, we may obtain the hypersurface relationship. The complexity of the MOO problem will be greatly increased. Therefore, we do not consider the influence of optimized variables to reduce the complexity of fitting. We adopt nonparametric regression method to fit the relationship between target variables. Then, a trade-off control surface for fuel economy, emission and drivability performance can be established.

To build the surface fitting relationship between the three objectives, it is necessary to convert these objectives into the dependent and the independent variables. Because of the obvious conflict between the objectives, emission and fuel economy are selected as the independent variables, while drivability is selected as the dependent variable. According to the sample data (Table 6), the curved surfaces are obtained with LOWESS method, as shown in Fig. 14.

The LOWESS method has two important parameters for fitting effect. One is the smoothing parameter ( $H$ ), also called window. It describes the ratio of observation number

and total data number within an interval. The greater the  $H$  value is, the smoother the fitting surface becomes. The other is the order of fitting polynomials ( $P$ ).  $P$  is usually set to be 0, 1, or 2. When  $P = 0$ , local polynomial estimation is same as the kernel estimation. When  $P = 1$ , any window is fitted to be a straight line. When  $P = 2$ , each window can be fitted to be a curve. Obviously, the higher the order of fitting polynomials is, the smoother does the curve change, but the fitting process becomes more and more complicated. In this paper, the order of fitting polynomials ( $P$ ) is set to be 1. In addition, the effect of the smoothing parameter on the fitting results is greater than the order of the fitting polynomial. Therefore, different smoothing parameters need to be adopted to fit the surface. While other parameters such as order of fitting polynomials can be set to be the default value, in this paper the smoothing parameters are set to be 10, 20, 30, 40, 50, 60, 70 and 100%, respectively. The corresponding effect of surface fitting is shown in Fig. 14.

It can be seen from Fig. 14a, b that the effect of the curved surface is not ideal. The reason is that the selected smoothing parameter is small. Although the fitting error is small, the smoothness still needs to be further improved. However, the smoothness may be damaged during surface fitting to reduce the fitting error. What is worse, some fitted points of surface may exceed the range of the coordinate axis.

As shown in Fig. 14c, when smoothing parameter  $H$  reaches 30%, the smoothness is greatly enhanced. The

**Table 6** Sample data

No.	$f_1$ (g/km)	$f_2$ (L/km)	$f_3$ (m/s <sup>3</sup> )	No.	$f_1$ (g/km)	$f_2$ (L/km)	$f_3$ (m/s <sup>3</sup> )
1	9.29	13.45	137.56	11	6.05	9.16	165.48
2	10.15	13.89	135.39	12	11.38	14.59	133.12
3	9.33	13.39	138.63	13	5.93	9.66	157.54
4	6.05	9.15	165.53	14	11.23	14.86	133.62
5	12.51	16.36	129.01	15	9.62	13.53	137.54
6	12.25	16.20	129.10	16	8.91	12.45	142.53
7	6.74	11.10	145.87	17	9.62	13.52	136.56
8	6.10	9.06	166.48	18	10.79	13.56	133.73
9	6.88	11.08	144.69	19	12.32	15.83	129.33
10	5.96	9.19	164.27	20	11.36	14.71	130.66
21	12.09	16.17	129.28	31	13.13	136.88	10.06
22	9.60	13.64	136.29	32	13.14	134.12	10.29
23	11.87	15.57	129.65	33	12.58	138.81	9.50
24	12.24	16.46	128.99	34	9.43	158.41	5.85
25	7.30	11.34	144.30	35	12.11	144.25	8.60
26	8.55	12.69	140.47	36	9.47	159.34	5.84
27	12.33	16.26	129.03	37	12.33	143.77	8.17
28	9.26	12.97	138.70	38	12.98	139.49	8.37
29	6.81	11.31	145.07	39	10.62	147.87	6.34
30	5.84	9.40	158.77	40	9.29	195.48	5.95

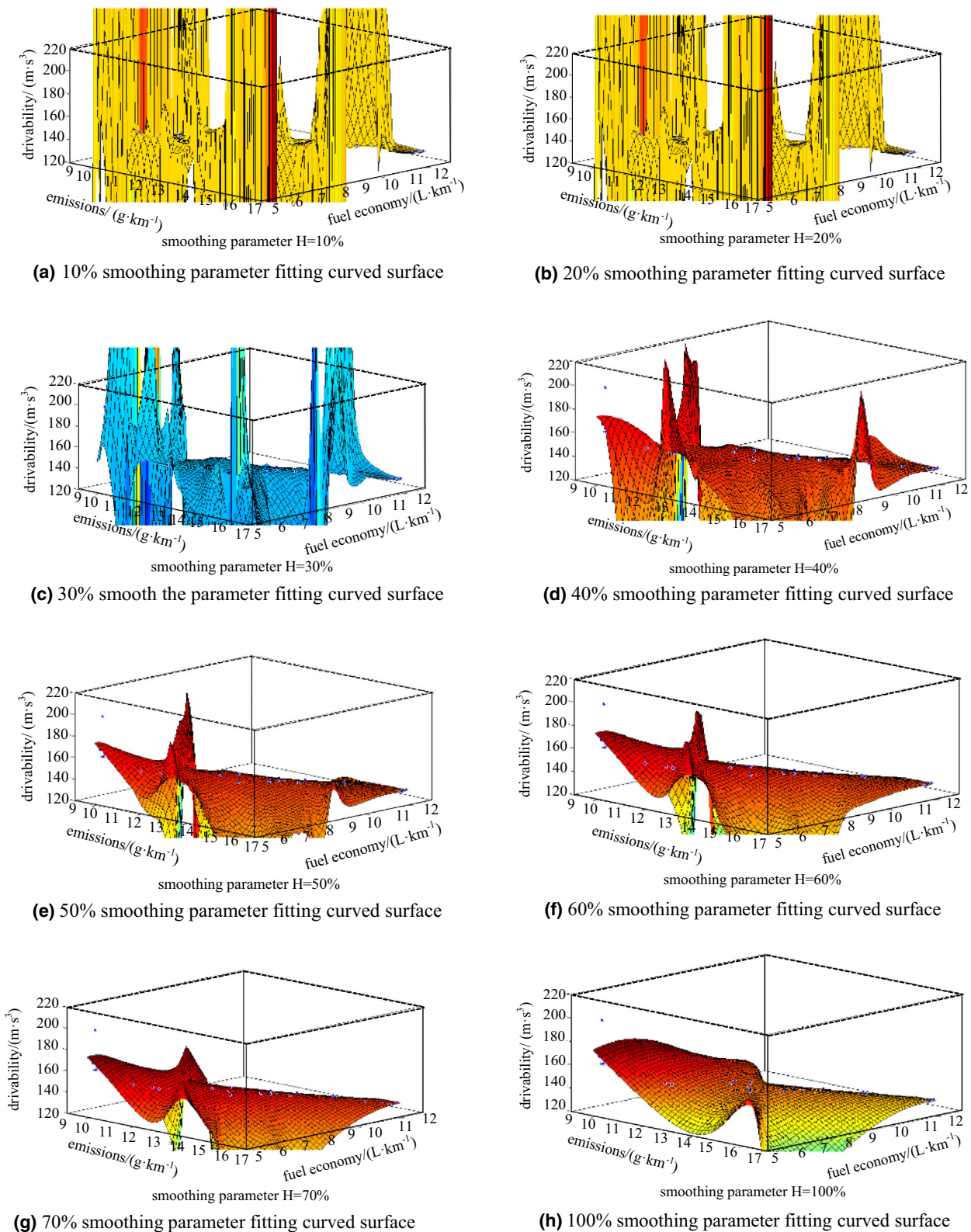


Fig. 14 Fitting curved surface for different smoothing parameter



numbers of fitted points exceeding the range of coordinate axis are greatly declined, but the error of surface fitting is greatly increased.

As shown in Fig. 14d, when the smoothing parameter  $H$  increases up to 40%, the effect of surface fitting is further improved. The change trend of entire surface gets more and more smooth. The fitting error just increases a little compared with Fig. 14c ( $H = 30\%$ ).

It can be seen from Fig. 14e–h that the effect of surface fitting also becomes much more and more smooth. Almost all fitting points are within the range of the coordinate axis. However, the fitting error becomes larger and larger. Obviously, there is a conflict between smoothness and fitting error. It is very significant to obtain a smoother curved surface with reasonably acceptable error through further study.

The above analysis focuses on qualitative illustration. To further evaluate the effect of surface fitting, we adopt the quantitative analysis method. We select sum of squares due to error (SSE), coefficient of determination ( $R$ -square), degrees of freedom (DFE), degree-of-freedom adjusted coefficient of determination (Adj  $R$ -sq), and root mean squared error (RMSE) as the performance indexes to evaluate the effect of surface fitting. The closer SSE is to 0, the better is the effect of surface fitting. On the contrary, the closer  $R$ -square or Adj  $R$ -sq is to 1, the better is the effect of surface fitting. The smaller DFE is, the better is the effect of surface fitting. The smaller the RMSE, which means the smaller error, the more closer is the fitting value to the real value. According to Fig. 14, the above five performance indexes can be computed and concluded as shown in Table 7.

As shown in Table 7, when  $H$  increases gradually, SSE becomes larger, while  $R$ -square, DFE and Adj  $R$ -sq show a gentle change. The fitting surface becomes more and more smooth. However, the effect of surface fitting becomes better in the beginning, but then rapidly declines. Especially when  $H$  varies between 20 and 30%, this downtrend is more obvious. When  $H$  is equal to 20%,  $R$ -square reaches a maximum value (0.998). Adj  $R$ -sq also gains optimal value (0.997). At this moment, the effect of surface fitting is best and the fitting error is the smallest. But the smoothness is not good and even some fitted points exceed the effective range. When  $H$  is closer to 30%, SSE, DFE and RMSE show a great change. The fitting error increases rapidly. When  $H$  changes from 30 to 100%, the smoothness changes better and better, and the fitting error becomes larger and larger at the same time. Obviously, the results of quantitative analysis can verify the qualitative conclusions.

In summary, the obtained fitted surface can reflect the distribution of the optimal solutions to some extent. The undiscovered optimal solutions can be predicted according to the change rule of the fitted surface. Through the

**Table 7** Fitting performance indexes

$H$ parameter %	SSE	$R$ -square	DFE	Adj $R$ -sq	RMSE
10	18.87	0.89	28	0.997	0.82
20	18.87	0.998	28	0.997	0.82
30	559.92	0.93	31.33	0.91	4.23
40	767.02	0.90	33	0.89	4.82
50	962.22	0.88	34	0.86	5.32
60	983.43	0.88	34.67	0.86	5.33
70	988.29	0.88	35.14	0.86	5.30
80	1007.03	0.87	36	0.86	5.29
90	1006.88	0.87	35.78	0.86	5.30
100	1007.03	0.87	36	0.86	5.29

existing results, the continuous change relationship between the fuel economy, emission and drivability can be established. The trade-off Pareto optimal control curved surface can be constructed. According to the performance requirements of the design, the appropriate control points can be selected based on the curved surface. Moreover, the rationality of the established optimal control strategy can also be evaluated by the fitting surface.

## 6 Conclusions

In this paper, the non-dominated sorting differential evolution algorithm (NSDEA) is proposed for the multi-objective optimization problem. Then, the locally weighted scatter plot smoothing (LOWESS) method is adopted to fit the Pareto optimal solutions to obtain the trade-off control curved surface.

1. Aiming at the multi-objective optimization for HEV, the fuel economy, emission and drivability are taken as optimization objectives. The control parameters which can greatly influence target variables are selected as optimization objects. Then the mathematical model of multi-objective optimization problem for HEV is established with constraints of dynamic performance and charge balance.
2. Combined with NSGA-II and DE algorithm, NSDEA is proposed to solve the multi-objective optimization problem. Multi-groups of Pareto solution sets with good distribution and convergence are obtained.
3. The NSDEA simulation results under UDDS cycle show that the evaluation index of fuel economy declines by 20.26% on average. The evaluation index of emission is improved by an average of 11.33%, and the maximum value of CO reaches 21.9%. The evaluation index of drivability is optimized by



20.84% on average, and the maximum value reaches 40.32%. All the evaluation indexes of fuel economy, emission and drivability are enhanced. Moreover, the obtained multi-groups of Pareto optimal solution sets are reasonable and effective.

4. To reduce the searching and calculating complexity of optimal solutions, the LOWESS method is adopted to fit the Pareto optimal solutions. The multi-objective trade-off control curved surface is finally obtained. It can guide energy management for the actual vehicle.

**Acknowledgements** This work was supported by the National Natural Science Foundation of China (Grant no. 51305473); Project Funded by China Postdoctoral Science Foundation (Grant no. 2014M552317); Postdoctoral Science Funded Project of Chongqing (Grant no. xm2014032). Finally, the authors are grateful to the anonymous reviewers for their helpful comments and constructive suggestions.

### Compliance with ethical standards

**Conflict of interest** The authors declare no conflict of interests, including specific financial interests and relationships relevant to the subject of this paper.

### References

1. Zhang BZH (2011) Study on energy management control strategy for plug-in hybrid electric vehicle. Hefei University of Technology, Hefei, pp 33–57
2. Li XSH, Chen D, Zhou YJ (2012) Energy management strategy of hydraulic hybrid vehicle based on instantaneous equivalent fuel consumption minimization. *J Highw Transp Res Dev* 29(12):148–152
3. Qin DT, Zeng YP, Su L et al (2015) Plug-in hybrid vehicle's real-time control strategy based on approximate Pontryagin's minimum principle. *J Mech Eng* 51(2):134–140
4. Zou Y, Hou SHJ, Han EL et al (2012) Dynamic programming-based energy management strategy optimization for hybrid electric commercial vehicle. *Automot Eng* 34(8):663–668
5. Xiao RX, Li T, Zou G et al (2013) Energy management strategy for series-parallel hybrid electric vehicle based on stochastic dynamic programming. *Automot Eng* 35(4):317–321
6. Galvagno E, Morina D, Sorniotti A et al (2013) Drivability analysis of through the road parallel hybrid vehicles. *Meccanica* 48(2):351–366
7. Patrick W (2011) Plug-in hybrid electric vehicle supervisory control strategy considerations for engine exhaust emissions and fuel use. Virginia Polytechnic Institute and State University, Virginia, pp 44–125
8. Yue MY, Zhou YD, Ma G (2015) Research progress on deep hybrid vehicle NVH problem. *Mach Des Manuf* 2:268–271
9. Zheng HY, Wang LL, Zhao WQ et al (2015) Braking force distribution control strategy of bus based on electronically controlled braking system. *J Jilin Univ* 45(2):347–351
10. Qin DT, Wei HB, Duan ZHH et al (2012) Multiple-objective real-time optimum control strategy for fuel consumption and emission of full hybrid electric vehicle. *J Mech Eng* 48(6):83–89
11. Pierre M, Alain C, Guillaume C et al (2012) Energy management of HEV to optimize fuel consumption and pollutant emissions. In: 11th international symposium on advanced vehicle control, AVEC'12, Seoul, South Korea
12. Wang Q, Frank A (2014) Plug-in HEV with CVT: configuration, control, and its concurrent multi-objective optimization by evolutionary algorithm. *Int J Automot Technol* 15(1):103–115
13. Shashi A, Wang G, An Q et al (2012) Using the Pareto set pursuing multi-objective optimization approach for hybridization of a plug-in hybrid electric vehicle. *J Mech Des* 134(9):503–509
14. Dongsuk K, Huei P, Norman K (2011) Optimal catalyst temperature management of plug-in hybrid electric vehicles. In: American control conference on O'Farrell Street, San Francisco, CA, USA
15. Dongsuk K, Huei P, Norman B (2006) Supervisory control of parallel hybrid electric vehicles for fuel and emission reduction. *ASME J Dyn Syst Meas Control* 133(061010):1–10
16. Daniel O, Wang XY, Ryan M (2011) An energy management controller to optimally trade off fuel economy and drivability for hybrid vehicles. *IEEE Trans Control Syst Technol* 12(11):1–16
17. Daniel O, Wang XY, Ryan M (2012) An energy management controller to optimally trade off fuel economy and drivability for hybrid vehicles. *IEEE Trans Control Syst Technol* 20(6):1490–1505
18. Deng T, Lin CHS, Li YN et al (2015) A multi-objective optimization method for energy management control of hybrid electric vehicles using NSGA-II algorithm. *J Xi'an Jiaotong Univ* 49(10):143–150
19. Yang GC, Li SHB, Qu JL et al (2012) Multi-objective optimization of hybrid electrical vehicle based on Pareto optimality. *J Shanghai Jiaotong Univ* 46(8):1297–1303
20. Zeng XH, Wang QN, Wang WH (2007) Modelling and simulation of energy loss minimization for hybrid electric vehicle. *J Syst Simul* 19(18):4309–4325
21. Musardo C, Rizzoni G, Staccia B (2005) A-ECMS: an adaptive algorithm for hybrid electric vehicle energy management. *Eur J Control* 11(4–5):509–524